



1 Responses of fossil coccolith morphology to preservation
2 conditions in the deep ocean

3 Authors: Amanda Gerotto^{1,3*}, Hongrui Zhang^{2*}, Renata Hanae Nagai³, Heather M. Stoll², Rubens
4 César Lopes Figueira¹, Chuanlian Liu⁴, Iván Hernández-Almeida²

5 ¹Oceanographic Institute, University of São Paulo, São Paulo, Brazil; ²Geological Institute, ETH
6 Zurich, Zurich, Switzerland; ³Center for Marine Studies, Federal University of Paraná, Pontal do
7 Paraná, Brazil; ⁴State Key Laboratory of Marine Geology, Tongji University, Shanghai, China.

8 *Corresponding authors: gerottoamanda@alumni.usp.br, zhh@ethz.ch

9

10 Abstract

11 Understanding the variations in past ocean carbonate chemistry is critical in elucidating the role
12 of the oceans in balancing the global carbon cycle. The fossil shells from marine calcifiers present
13 in the sedimentary record are widely applied as past ocean carbon cycle proxies. However, the
14 interpretation of these records can be challenging due to the complexity physiological and
15 ecological response to the carbonate system during organisms' life cycle, as well as the potential
16 for preservation at the sea-floor. Here we present a new dissolution proxy based on the
17 morphological attributes of coccolithophores from the Noëlaerhabdaceae family (*Emiliania*
18 *huxleyi* and *Gephyrocapsa* spp., > 2 μm). To evaluate the influences of coccolithophore
19 calcification and coccolith preservation on fossil morphology, we measured morphological
20 attributes, mass, length, thickness, and shape factor (ks), of coccoliths in a laboratory dissolution
21 experiment and surface sediment samples in the South China Sea. The coccolith morphological
22 data in surface sediment were also analyzed with environment settings, namely surface
23 temperature, nutrients, pH, chlorophyll-a concentration, and carbonate saturation of bottom
24 water by a redundancy analysis. Statistical analysis indicate that carbonate saturation of the
25 deep ocean explains the highest proportion of variation in the morphological data instead of the
26 environmental variables of the surface ocean. Moreover, the dissolution trajectory in the ks vs
27 length of coccoliths is comparable between natural samples and laboratory dissolution
28 experiments, emphasizing the importance of carbonate saturation on fossil coccolith
29 morphology. However, the mean ks alone cannot fully explain all variations observed in our
30 work. We propose that the mean ks and standard deviation of ks (σ) over the mean ks (σ/ks)
31 could reflect different degrees of dissolution and size-selective dissolution, influenced by the
32 assemblage composition. By applying together with the σ/ks ratio, the ks factor of fossil
33 coccoliths in deep ocean sediments could be a potential proxy for a quantitative reconstruction
34 of past carbonate dissolution dynamics.



35

36 1. Introduction

37 The ocean's large reservoir capacity of carbon dioxide (CO₂) plays an essential role in the
38 carbon cycle and, consequently, in controlling atmospheric CO₂ (Ridgwell and Zeebe, 2005;
39 Wang et al., 2016). The ocean pCO₂ is influenced by temperature, salinity, and biological activity,
40 including primary production, respiration, calcification, and carbonate dissolution (Ridgwell and
41 Zeebe, 2005; Sarmiento and Gruber, 2006; Libes, 2009; Wang et al., 2016). When CO₂ dissolves
42 in water, the ocean becomes more acidic, decreasing pH, carbonate ion concentration,
43 carbonate saturation (Ω_{Ca}). The carbonate compensation depth (CCD) is the depth at which the
44 rate of calcite dissolution is balanced by the rate of calcite supply. The CCD is usually several
45 hundred meters deeper than the chemical lysocline, the saturation horizon of calcite, due to the
46 kinetics of dissolution (Ridgwell and Zeebe, 2005). Whereas the photic zone is supersaturated
47 with respect to calcite in most areas of the ocean, large areas of the deep ocean are currently
48 undersaturated because of the increased solubility of calcite with pressure (Sulpis et al., 2018).
49 As the ocean continues absorbing larger amounts of CO₂ from anthropogenic fuel emissions, a
50 shallowing of the CCD is expected for the next 100 years due to the sharp decrease of carbonate
51 saturation from surface to deep ocean (Hönisch et al., 2012; USGCRP, 2017; Sulpis et al., 2018;
52 IPCC, 2019). Variations in the CCD on timescales from millions to several thousands of years are
53 an important process in determining the ocean's carbonate chemistry and regulating
54 atmospheric CO₂ (Emerson and Archer, 1990; Pälike et al., 2006). Understanding the role of
55 physical and biogeochemical parameters in marine carbonates is therefore critical to interpret
56 the geological record correctly and to reconstruct variations of the ocean carbon cycle in the
57 past.

58 The effects of carbonate chemistry changes and variations in the position of the CCD in
59 the geological past have been investigated using a wide array of geochemical and microfossil
60 proxies such as $\delta^{13}C$ in benthic and planktonic foraminifera (Zachos et al., 2005; Hönisch et al.,
61 2012), fragmentation indices of calcareous microfossils (Le and Shackleton, 1992; Broerse et al.,
62 2000; Flores et al., 2003), and CaCO₃ content (Archer et al., 2000; Pälike et al., 2006) in marine
63 sediments. However, these proxies do not provide quantitative estimates of past changes in
64 carbonate chemistry because some additional ecological mechanisms determine the
65 calcification and preservation responses (Hönisch et al., 2012; Rae et al., 2021). $\delta^{11}B$ provides
66 quantitative proxy for past seawater pH (Hönisch et al., 2012), albeit additional carbonate
67 chemistry parameters impose some limits on the interpretation of the proxy (Yu and Elderfield,
68 2007; Rae et al., 2021). Benthic B/Ca provides a quantitative proxy for deep sea CO₃²⁻



69 concentration (Yu et al., 2016). Yet both of these methods require mono-specific foraminifera
70 samples for measurements, which are time-consuming to pick, and analyses are limited to
71 sediment samples that contain sufficient concentration of this microfossil group.

72 Coccolithophores, a group of single-celled calcifying algae, are characterized by the
73 production of calcite plates called coccolith. Coccoliths are the main constituent of marine
74 biogenic sediments, contributing up to 80 % to deep-sea carbonate fluxes (Young and Ziveri,
75 2000; Hay, 2004). Changes in coccoliths morphology were believed to record the evolution
76 history of coccolithophores and reflect the environmental conditions in the surface ocean (i.e.
77 during coccolith biomineralization) (Riebesell et al., 2000; Iglesias-Rodriguez 2008; Beaufort et
78 al., 2011; Charalampopoulou et al., 2016; Rigual-Hernández et al., 2020a). Because of that,
79 coccoliths are widely used in paleoclimate and paleoceanographic reconstructions (e.g., Rickaby
80 et al., 2007; Henderiks and Pagani, 2007; Bolton et al., 2016; Bollman and Herrle, 2007). Several
81 methods exist to estimate coccolithophore calcification in the fossil record. Assumed
82 proportional length and thickness allowed for the first estimates of coccolith mass using
83 microscope techniques (Young and Ziveri, 2000). More recent methods based on the optical
84 properties of calcite under polarized light microscopy (circular and linear) allowed a more
85 precise estimate of the thickness of individual coccoliths (Beaufort, 2005; Beaufort et al., 2021;
86 Bollman et al., 2014; Fuertes et al., 2014; Johnsen and Bollmann, 2020). The optical techniques
87 have been successfully employed in downcore records to estimate coccolithophore calcification
88 across time and evolutionary steps (e.g., Bolton et al., 2016; Beaufort et al., 2022; Guitián et al.,
89 2022). However, until now there is no study that evaluates the response of calcification patterns
90 of fossil coccolithophores to both environmental parameters controlling biomineralization in the
91 photic zone and calcite saturation state at the depth of burial.

92 The South China Sea (SCS) is the largest marginal basin of the Western Pacific,
93 characterized by very dynamic spatial environmental conditions and a steep bathymetric profile
94 (Wang et al., 2015). Sediment records from this basin have been used to study the response of
95 coccolithophores to different environmental variables. Previous studies found positive
96 correlations between coccolithophores biometry from plankton samples and nutrients and light
97 at the photic zone (Jin et al., 2016). Building up on these results, but applied to the sedimentary
98 record, Su et al. (2020) explored the dependency of coccolithophore weight and past surface
99 ocean carbon chemistry parameters and nutrient conditions. However, it has been also
100 demonstrated that there is intense coccolithophore dissolution above the lysocline in the SCS
101 (Fernando et al., 2007a). More recently, a study using plankton tow material found that the
102 degree of calcification in the coccolithophore species *Emiliania huxleyi* was insensitive to
103 carbonate chemistry in surface waters (Jin et al. 2022a). This diversity of results calls for new



104 studies that explore systematically the drivers of coccolithophore morphology and calcification
105 in the fossil record.

106 Here, we analyzed morphological attributes of fossil coccolithophores in surface
107 sediment samples ($n = 28$) in the SCS, located across spatial environmental gradients in the
108 surface ocean, but also across a bathymetric transect related to the calcite saturation at the sea
109 floor which leads to lower calcite saturation at the sea-floor in deeper sites. In addition, we
110 evaluated the morphological variations of coccoliths under different dissolution intensities in a
111 laboratory experiment. Using an automated algorithm to estimate coccolithophore calcification
112 from images taken with a microscope under cross-polarization, we show that scale-invariant
113 measures of coccolith thickness (shape factor, k_s) from coccolithophores located along a depth
114 gradient in the SCS are highly correlated to the calcite saturation state at the seafloor. We
115 propose a new calibration to reconstruct past calcite saturation based on k_s which would enable
116 the quantitative reconstruction of changes in the calcite saturation in the deep ocean and
117 position of the CCD in the past.

118

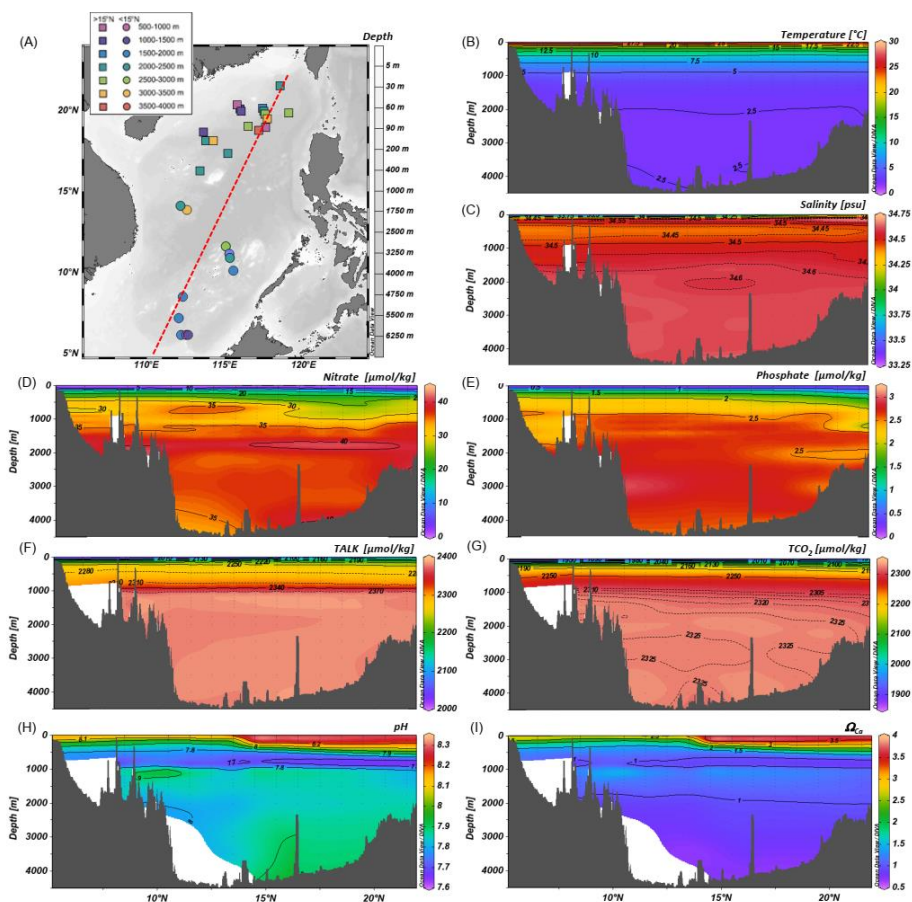
119 2. Oceanographic settings

120 The SCS is a marginal basin located in the Western Pacific, connected to the open ocean
121 by north and south shallow passages (Fig. 1A). The Luzon Strait in the north is the deepest (~ 2000
122 m) and the principal channel for water exchanges between the SCS and the Pacific through the
123 Kuroshio Current (Qu et al., 2006; Liu et al., 2011; Wan and Jian, 2014). The modern surface
124 circulation and hydrographic characteristics of the SCS are directly associated with the seasonal
125 changes promoted by the East Asian Monsoon (Wang and Li, 2009). These seasonal
126 hydrodynamic patterns control the regional sea surface temperature (SST) distribution, salinity,
127 and nutrients (Fig. 1B-E, Wang and Li, 2009). The SST latitudinal gradient is up to 2°C with an
128 annual average of $28\text{-}29^\circ \text{C}$ in the southern SCS and $26\text{-}27^\circ \text{C}$ in the north (Tian et al., 2010).
129 Salinity varies seasonally between 32.8-34.2 psu, with smaller salinity variation in the north than
130 in the south (Wang and Li, 2009). Northern SCS primary productivity reflects the seasonality of
131 the EAM with more productive and well-mixed waters during the winter season (Zhang et al.,
132 2016), with higher chlorophyll- a concentration ($0.65 \text{ mg Chl-}a \text{ m}^{-3}$ and $600 \text{ mg C m}^{-2} \text{ d}^{-1}$) (Chen,
133 2005; Chen et al., 2006; Jin et al., 2016).

134



135



136

137 Figure 1. Map of the South China Sea and location of core-top samples used in the present study.
138 Dots and squares represent stations located from 6° to 15° N, and from 15° to 22° N. (A). Vertical
139 profiles along N-S (5° to 22° N) transect (dotted red line on panel A) of (B) temperature, (C)
140 salinity, (D) nitrate, and (E) phosphate obtained from World Ocean Atlas 2001 (WOA01,
141 Conkright et al., 2002), (F) total alkalinity (TALK) and (G) total inorganic carbon concentration
142 (TCO₂) from Goyet et al. (2000), (H) pH and (I) Ω_{ca} calculated at CO2SYS (Pierrot et al., 2012)
143 from previously extracted data (Goyet et al., 2000). The map and the vertical profiles were
144 plotted with ODV software (Schlitzer, 2019).

145

146 The modern SCS lysocline is approximately 1200 m, and the CCD lies between 3500 and
147 3800 m (Thunell et al., 1992; Wang et al., 1995; Luo et al., 2018). In the northern SCS, surface
148 waters (e.g., the upper 300 m) are characterized by relatively lower DIC and TALK (Fig. 1F-G) and



149 higher pH and Ω_{Ca} , compared to deeper waters (Fig. 1H-I) (Chou et al., 2007; Jin et al., 2016).
150 Below 1000 m, the SCS across a N-S transect is characterized by relatively homogeneous DIC,
151 $\delta^{13}C$, and $[CO_3^{2-}]$ (Chen et al., 2006; Qu et al., 2006; Chou et al., 2007; Wan et al., 2020).

152 The SCS deep waters originate from the North Pacific Deep Water (NPDW) that
153 penetrates the marginal basin through the Luzon Strait (Qu et al., 2006; Liu et al., 2011; Wan
154 and Jian, 2014; Wan et al., 2018). The route traced from the Luzon Strait to the northwest
155 suggests a predominantly cyclonic deep circulation (Qu et al., 2006; Wang and Li, 2009). The
156 deep-water residence time of the SCS is estimated to be approximately 30-50 years, like that of
157 intermediate waters, 52 years (Chen et al., 2001). Due to this short residence time, the SCS
158 presents a homogeneous vertical profile; below 2000 m, there are no evident chemical
159 stratification or changes compared to the Pacific deep-water chemistry (> 2000 m)
160 characteristics (Chen et al., 2001; 2006; Qu et al., 2009). The rapid residence time potentially
161 implies that, when replaced, deep waters occupy intermediate water levels (between 300 m and
162 1300 m), contributing to the circulation of intermediate and shallow waters and ocean-
163 atmosphere exchanges (Qu et al., 2009; Tian et al., 2010).

164 3. Material and methods

165 3.1 Material and sample treatments

166 The core-top samples ($n = 28$) employed in this study were retrieved from different
167 depths in the basin of SCS (Fig. 1) during the R/V Sonne cruises (SO-95) (Table 1). Toothpick
168 samples from each location were used to prepare smear slides, without any chemical or physical
169 treatment. Unfortunately, the surface sediments were already depleted resulting in not having
170 enough material to perform dissolution experiment using the same samples. For the dissolution
171 experiment, we employed 240 mg of dry sediment obtained from the Late Pleistocene sample
172 from the Western Equatorial Pacific (ODP 807A-2H-2W, 57-59 cm). This sample contains a higher
173 abundance of the species *Gephyrocapsa caribbeanica* compared to the thinner species found in
174 the SCS (Roth and Coulbourn, 1982; Roth and Berger, 1975). The sediment sample was
175 suspended in 120 ml Milli-Q water, and then the suspension was evenly separated into 6
176 centrifuge tubes, each a volume of 20 mL and containing the equivalent of 40 mg of sediment.
177 Sodium hexametaphosphate ($NaPO_3)_6$ (Calgon®) has been traditionally used in pretreatment of
178 samples with calcareous microfossils, particularly foraminifera (Olson and Smart 2004; Smart et
179 al., 2008). However, it has been observed that application of this chemical agent dissolves these
180 microfossils due to complexation of Ca with phosphates, an effect which varies with the
181 exposure time (Feldmeijer et al., 2013). Therefore, we added 100 mg of Calgon® into 100 ml
182 Milli-Q water, resulting in a concentration of 1.6mM, to conduct our dissolution experiment.



183 Different volumes of Calgon® solution (0, 0.4, 0.8, 2, 4 6 ml) were added to each of the six
184 subsamples. The Calgon® is very corrosive to the fine carbonate particles, and the reaction
185 between Calgon® and carbonate could be simplified in two steps. First, the $(\text{NaPO}_3)_6$ hydrolysis
186 releases the sodium trimetaphosphate ($\text{Na}_3\text{P}_3\text{O}_9$). Then, the calcium in the solution is exchanged
187 with sodium and precipitate as $\text{Ca}(\text{PO}_3)_2$, $\text{CaNa}(\text{PO}_3)_3$, and $\text{CaNa}_4(\text{PO}_3)_6$, strongly reducing the free
188 calcium concentration in the solution. The decrease in calcium concentration promotes
189 carbonate dissolution. In theory, adding 1 mol $(\text{NaPO}_3)_6$ would result in the dissolution of 3 mol
190 CaCO_3 at maximum. So, there could be ~80 % carbonate left even after adding 6 ml Calgon®
191 solution. The particles in all tubes were kept suspended gently by a rotating disaggregation
192 wheel as described previously (Stoll and Ziveri, 2002) for two days to achieve a full reaction
193 between carbonate and $(\text{NaPO}_3)_6$. Slides were prepared for coccolith morphological analyses
194 using the drop technique as described by Bordiga et al. (2015) to trace the variations of coccolith
195 amount during dissolution.

196

197 3.2 Coccolith morphological parameters

198 The morphological parameters of coccolith in the dissolution experiment and surface
199 sediment were analyzed using a Polarized Microscope (Zeiss Axio Scope HAL100), configured
200 with circularly polarized light and a Zeiss Plan-APOCHROMAT 100x/1.4 oil objective, and a
201 coupled camera (Zeiss AxioCam 506 Color). For every sample, at least 40 fields of view were
202 photographed. After species identification and selection of coccolithophore images belonging
203 to the Noëlaerhabdaceae family (*Emiliana huxleyi* and *Gephyrocapsa* spp, $> 2 \mu\text{m}$), each sample
204 had between 100 and 400 (average of 250 per sample) coccolithophore images. The relationship
205 between the color of coccolith images and thickness was calibrated using a reference calcite
206 wedge, the thickness of which had been carefully quantified (González-Lemos et al., 2018). After
207 calibration, all images were analyzed in the Matlab-based software, C-Calcita (Fuertes et al.,
208 2014), to obtain the coccolith morphological parameters, including length, volume, and mass.
209 The length-shape factor of each coccolith, k_s , was calculated using the formulation by Young and
210 Ziveri (2000) based on the coccolith mass and length obtained using C-Calcita:

$$211 k_s = \frac{\text{Mass}}{2.7 \times \text{Length}^3}$$

212

213 Beyond the traditional morphological parameters, we calculated the ratio of the
214 standard deviation of k_s (σ) over the mean k_s (σ/k_s). The goal of this novel parameter is to
215 provide a new dimension to trace the dissolution process in coccoliths, especially when the
216 coccolith assemblage is diverse. For example, if the coccoliths dissolve at different speeds in the



217 assemblage due to differential sensitivity to acidification, a small increase of σ/ks would be
218 expected at the beginning of the dissolution because of the σ increase and ks decrease. Then,
219 after all fragile coccoliths dissolve, leaving only thicker coccoliths in the assemblage, the σ/ks
220 should show a decreasing trend which could be mainly caused by a decrease σ .

221

222 Table 1. Station, coordinate data, and water depth of core-top samples used in this study.

Station	Longitude (E)	Latitude (N)	Water depth (m)
17930	115.782	20.333	629
17965	112.552	6.157	889
17943	117.553	18.95	917
17931	115.963	20.1	1005
17944	113.637	18.658	1219
17963	112.667	6.167	1233
17932	116.037	19.952	1365
17964	112.213	6.158	1556
17960	115.558	10.12	1707
17940	117.383	20.117	1728
17961	112.332	8.507	1795
17959	115.287	11.138	1957
17962	112.082	7.182	1970
17949	115.167	17.348	2195
17957	115.31	10.9	2197
17941	118.483	21.517	2201
17951	113.41	16.288	2340
17945	113.777	18.127	2404
17955	112.177	14.122	2404
17939	117.455	19.97	2473
17958	115.082	11.622	2581
17934	116.462	19.032	2665
17938	117.538	19.787	2835
17925	119.047	19.853	2980
17956	112.588	13.848	3387
17937	117.665	19.5	3428
17946	114.25	18.125	3465



17936 117.12 18.767 3809

223

224

225 3.3 Environmental data for surface sediment

226 Annual means of different physical, chemical and biological variables in both 50 m depth
227 and bottom water for the location of the surface samples (Table 1) were extracted from different
228 databases. Here the 50 m depth was selected because it is the depth at which the highest
229 concentration of Noëlaerhabdaceae coccolithophorid has been observed in the SCS (Jin et al.,
230 2016). Seawater temperature, salinity, phosphate, and nitrate concentrations at 50 m were
231 obtained from WOA01. Sea surface chlorophyll-a concentration data were based on MODIS data
232 (2003-2016) extracted from Oregon State University Ocean Productivity
233 (<http://www.science.oregonstate.edu/ocean.productivity/>). Annual averaged concentrations of
234 total alkalinity (TALK) and dissolved inorganic carbon (TCO₂) were extracted from Goyet et al.
235 (2000). Then the carbonate ion concentration, pH, pCO₂ for the depth of 50 m and Ω_{Ca} for the
236 sea floor depth were calculated by CO2SYS macro for Excel® (Pierrot et al., 2012) using extracted
237 variables, salinity, temperature, pressure, total phosphate, total silicate, TALK, and TCO₂ at the
238 corresponding depth (50 m or depth of the surface sediment sample). The light intensity at 50
239 m water depth was calculated using a model of penetration of photosynthetic active radiation
240 (PAR) from surface to depth (Buiteveld, 1995; Murtugudde et al., 2002), monthly climatologies
241 of PAR from the MODIS Ocean database (<http://oceancolor.gsfc.nasa.gov/cgi/l3>), and the
242 diffuse attenuation coefficient for downwelling irradiance at 490 nm (Kd490) and Equation 1 in
243 Lin et al. (2016).

244

245 3.4 Statistical analysis

246 Pearson correlation and redundancy analysis (RDA) were employed to explore the
247 relationship between morphological features of the coccoliths in surface sediment samples and
248 the environmental data. All statistical analyses were performed using the PAST 4.06 software
249 (Hammer et al., 2001).

250

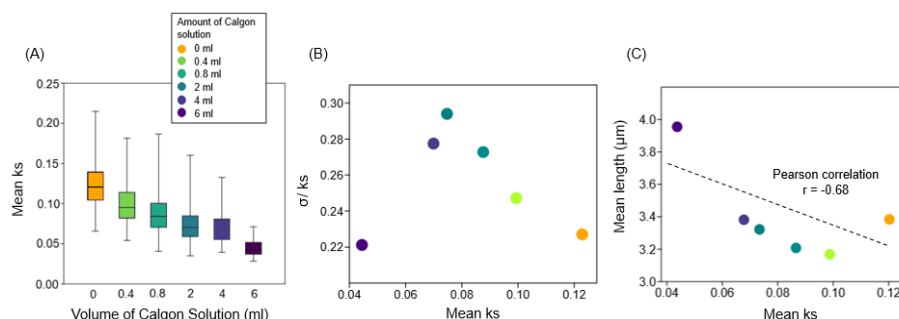
251 4. Results

252 4.1 Variations of coccoliths morphology in the dissolution experiment

253 In the dissolution experiment, mean ks decreased with increasing volume of Calgon®
254 solution (Fig. 2A). The mean ks varied between 0.12 (0 ml Calgon®) and 0.04 (6 ml Calgon®) (Fig.
255 2A). The σ/ks represents variation in preservation among coccoliths within each sample. Higher



256 differences in σ were observed in samples containing 2 ml, 4 ml, 0.8 ml, 0.4 ml, 0 ml, and 6 ml,
 257 respectively (Fig. 2B). Increasing the amount of Calgon® solution up to 2 ml showed a decrease
 258 in mean k_s and an increase in σ . Samples with 4 and 6 ml Calgon® solution showed a reduction
 259 in mean k_s and σ among coccoliths (Fig. 2B). The lowest mean k_s (0.04) and the maximum mean
 260 length (3.95 μm) were recorded under the higher Calgon® solution (6 ml) amount (Fig. 2C).
 261 Increased amounts of Calgon® solution also resulted in a gradual increase in coccolith length
 262 leading to a negative correlation between length and k_s ($r = -0.68$, $p > 0.05$), but not significant
 263 due to the small number of observations (Fig. 2C).

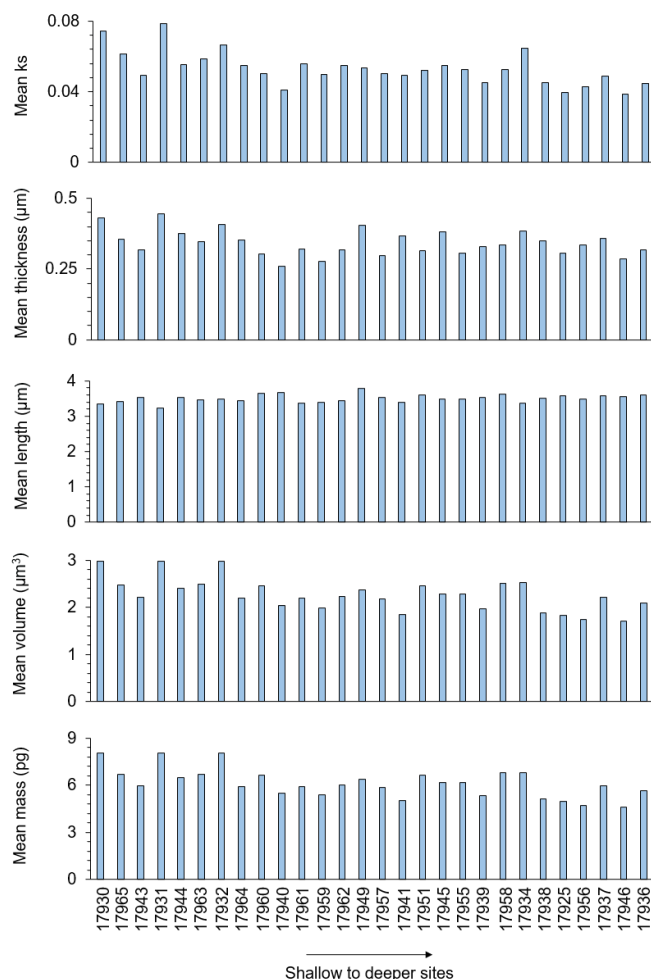


264
 265 Figure 2. Coccolith morphological variations in the dissolution experiment. (A) Box plots of the
 266 median (horizontal line inside the boxes), minimal and maximal values of coccoliths mean k_s
 267 (vertical bars) under the different volumes of Calgon® solution; (B) Scatter plot of mean k_s and
 268 σ/k_s and (C) linear correlation and correlation coefficient ($p > 0.05$) between mean k_s and mean
 269 length.

270

271 4.2 Biological and environmental effects on coccolith morphology

272 Overall, the mean k_s , thickness, and volume in the core-top sampling stations (Fig. 3)
 273 presented higher values in shallower depths. The mean k_s varied between 0.03 and 0.07, and
 274 the mean thickness was between 0.25 and 0.44 μm , with maximum values recorded at station
 275 17931 located in northern SCS at 1005 m water depth. The mean length of coccolith varied
 276 between 3.23 and 3.78 μm , with the highest values recorded at 2195 m water depth (site 17949)
 277 in northern SCS, but without a significant trend along depths. The mean volume of coccoliths
 278 ranged between 1.70 and 2.97 μm^3 , and the mean mass was between 4.61 and 8.03 μg , with
 279 maximum values for both recorded in the shallowest station, 17930, at 629 m water depth in
 280 northern SCS.



281

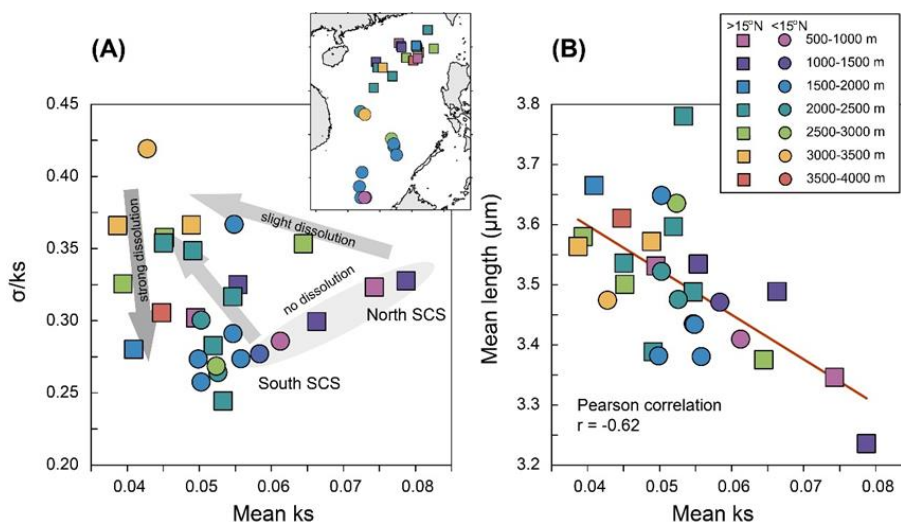
282 Figure 3. Cocolith mean ks, thickness (μm), length (μm), volume (μm^3), and mass (pg) in surface
283 samples from SCS. The sampling stations are distributed along the x-axis according to their
284 depth, sorted from the shallowest to the deepest.

285

286 In general, the degree of dissolution varied according to the depth of the sediment
287 samples. The σ/ks vs. ks presents different trajectories associated with light, strong, or no
288 dissolution (Fig. 4A). The shallowest stations south ($<15^\circ \text{N}$) and north SCS ($>15^\circ \text{N}$) show a linear
289 and increasing trend between ks and σ/ks . For the samples below 2000 m, there is no clear
290 pattern of variation related to the mean ks standard deviation. However, samples below 3000
291 m are mainly located on the left upper part of the plot, in a similar position as the samples
292 treated with 4 and 6 ml of Calgon® in the ks vs. σ/ks comparison of the dissolution experiment



293 (Fig. 3B). The mean k_s vs. mean length shows a negative correlation ($r = -0.62$, $p < 0.05$), with
294 the deepest samples showing larger size coccoliths and lower mean k_s (Fig. 4B).
295
296



297
298 Figure 4. Morphological parameters of coccolith in surface sediments (A) Scatter plot between
299 mean k_s and σ/k_s and (B) linear correlation and correlation coefficient ($p < 0.05$) between mean
300 k_s and mean length. Shaded arrows in panel A represent ideal trajectories of mean k_s vs σ/k_s as
301 shown in figure 2B, to interpret the trends in the surface sediment samples. Note that the mean
302 k_s of figures 2 and 4 are different due to the higher abundance of the species *Gephyrocapsa*
303 *caribbeanica*, with higher thickness, in the sample for the dissolution experiment.

304

305 We analyzed the correlations between the biological and environmental datasets (Table
306 2). Significant correlations can be found ($p < 0.05$) between several morphological parameters
307 of coccolith and bottom water carbonate chemistry (Ω_{Ca}), with a correlation coefficient (r) = 0.67
308 between mean k_s and Ω_{Ca} , $r = 0.66$ between mean volume and Ω_{Ca} , and $r = 0.66$ between mass
309 and Ω_{Ca} . The mean thickness of the coccolith shows a significant correlation with Ω_{Ca} at the
310 sample depth ($r = 0.41$), and with the concentrations of nutrients nitrate and phosphate at 50 m
311 ($r = 0.44$ and 0.4 , respectively). Surprisingly, the mean length showed no significant correlation
312 to any environmental variables except with PAR ($r = 0.35$).

313 The results of RDA can provide another critical perspective on the control of
314 environmental variables on coccolith morphology. The RDA1 and RDA2 explain together 58.3 %
315 of the total variations in coccolith morphological data. The surface sediment samples, color-



316 coded by different depth intervals, are distributed along the axis of RDA1, which is the most
 317 important and explains 54.6 % of the total variance (Fig. 5A). Among the environmental
 318 variables, Ω_{Ca} shows the highest correlation to RDA1 ($r = -0.67$, $p < 0.05$). The results of both the
 319 correlation analyses and the RDA show that Ω_{Ca} in bottom water is the most important
 320 environmental variable driving the morphological dataset, which shows a high correlation with
 321 mean ks ($r = 0.69$; $p < 0.05$) and could explain up to 47 % ($R^2 = 0.47$) of the variance observed in
 322 mean ks (Fig. 5B). The RDA2 explained 3.69 % of the variance and is mainly correlated to the
 323 salinity, temperature, pH, phosphate, TALK, and pCO_2 (Fig. 5A). The null response of coccolith
 324 length to any environmental parameter is also observed in the RDA plot by its position near the
 325 center of the ordination space, significantly contrasting with other morphological parameters
 326 (Fig. 5A).

327

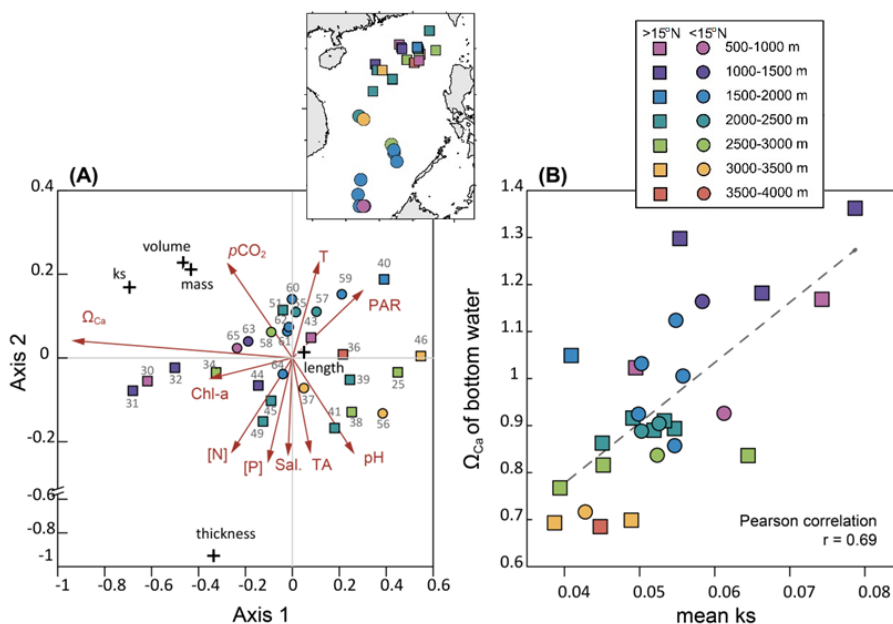
328 Table 2. Correlation matrix (p-value and Pearson correlation) between biological and
 329 environmental variables. Bold values indicate significant correlations (with $p < 0.05$).

Environmental/ Biological	p value					r				
	Mean ks	Mean thickness	Mean length	Mean volume	Mean mass	Mean ks	Mean thickness	Mean length	Mean volume	Mean mass
Salinity	0.79	0.07	0.87	0.86	0.86	-0.05	0.34	0.03	-0.03	-0.03
Temperature	0.94	0.04	1.0	0.90	0.90	-0.01	-0.39	0.00	-0.02	-0.02
Phosphate	0.88	0.03	0.63	0.96	0.96	0.03	0.41	-0.09	-0.01	-0.01
Nitrate	0.36	0.02	0.30	0.71	0.71	0.17	0.44	-0.20	0.07	0.07
TALK	0.53	0.13	0.70	0.60	0.60	-0.12	0.28	0.07	-0.10	-0.10
Chlorophyll-a	0.26	0.18	0.88	0.18	0.18	0.22	0.25	-0.02	0.26	0.26
PAR	0.28	0.05	0.06	0.50	0.50	-0.21	-0.38	0.35	-0.13	-0.13
pH	0.18	0.31	0.38	0.24	0.24	-0.26	0.19	0.17	-0.22	-0.22
pCO_2	0.16	0.33	0.38	0.21	0.21	0.27	-0.19	-0.17	0.24	0.24
Ω_{Ca}	0.00	0.03	0.05	0.00	0.00	0.67	0.41	-0.36	0.66	0.66

330



331



332

333 Figure 5. Redundancy analysis (RDA) ordinations for environmental variables and morphological
334 measurements (A) and (B) linear correlation and correlation coefficient ($p < 0.05$) between Ω_{Ca}
335 at bottom depths and mean ks from surface samples.

336

337 5. Discussion

338 5.1 Comparisons between laboratory dissolution experiment and natural 339 samples

340

341 In this study, we evaluate fossil coccolith responses to dissolution under laboratory
342 experiments and field settings. In the dissolution experiment, ks values are higher than the
343 modern coccoliths in the SCS due to the higher abundance of the relatively thicker *G.*
344 *caribbeanica* in the downcore sediment sample. Though the absolute values of ks cannot be
345 directly compared between the dissolution experiment (Fig. 2B) and surface sediments (Fig. 4A),
346 the trajectory of morphological variations during the dissolution experiment does provide
347 important diagnostic information to explain phenomena observed in the surface sediment
348 samples.

349 First, the phenomenon that coccolith length increased with the decrease of ks could be
350 observed in both the dissolution experiment (Fig. 2C) and natural surface sediments (Fig. 4B).



351 The laboratory experiment showed that under controlled conditions (known changes in water
352 chemistry and uniform species composition), the coccolith morphology variations (mean length
353 and mean k_s) reflected different degrees of dissolution. We also observed a length-related
354 dissolution pattern, where smaller coccoliths gradually dissolve with the increase in Calgon®
355 concentration, leading to a higher average length but a lower mean k_s . The mean k_s and mean
356 length relationships in the surface samples (Fig. 4B) show a similar trend to the laboratory
357 observations (Fig. 2C). Thus, the observed trend and the largest size and lowest k_s in the surface
358 sediment samples are explained by the dissolution of the smallest species due to the lower Ω_{Ca}
359 at the deepest samples and increasing the abundance of the larger coccoliths.

360 Second, changes in the σ/k_s ratio in the dissolution experiment a slight and gradual
361 increase in dissolution and then a decrease with the highest concentrations of Calgon® (Fig. 2C).
362 In the laboratory experiment, the subsample with no Calgon® solution presented well-preserved
363 coccoliths with high mean k_s and a small standard deviation. As the amount of Calgon® solution
364 added to each subsample increases, small coccoliths start dissolving preferentially, decreasing
365 the mean k_s and increasing the standard deviation (Fig. 2B). With higher amounts of Calgon®
366 solution (4 and 6 ml), the small coccoliths are completely dissolved, resulting in an assemblage
367 dominated by larger coccoliths (Fig. 2C). Under these highest dissolution stages, the larger
368 coccoliths are also partially dissolved then both mean k_s and σ decrease (Fig. 2B). In this way,
369 the σ reflects how differential dissolution size selection affects the composition of the
370 assemblages. Hence, samples that are more (less) susceptible to dissolution result in more
371 homogeneous (heterogeneous) assemblages regarding carbonate preservation.

372 However, the trajectory of σ/k_s vs. k_s in surface sediments seems more complex than in
373 the dissolution experiment (Fig. 4A). First, there is a group of samples with a positive correlation
374 between σ/k_s and k_s from shallow areas of the north and south SCS. The depth of samples from
375 northern and southern SCS regions is similar, so we argue that this feature is not caused by
376 dissolution but due to the species differences in both parts of the SCS. The coccolithophores
377 have multi-stage blooms in the north SCS, with a peak of *G. oceanica* in late winter, when
378 coccolithophore fluxes are highest due to strong water column mixing and renewed nutrient
379 inventory, and another of *E. huxleyi* in early spring (Jin et al., 2019; Chen et al., 2007). In
380 contrast, *E. huxleyi* is the dominant species in the more oligotrophic south SCS (Fernando et al.,
381 2007b) due to its higher competitiveness in situations of lower nutrient concentration
382 (particularly nitrate) compared to *G. oceanica* (Eppley et al., 1969). So, even without any
383 influence from dissolution, the coccolith in the north SCS should feature a higher species
384 diversity and, thereby, a higher σ/k_s compared with the coccolith in the south SCS. Hence, the
385 variety of the coccolith assemblages in the surface sediment samples results in different



386 trajectories in σ/ks vs. ks plotting. But the general trend of σ/ks vs. ks in surface sediment is still
387 following the trends observed in the dissolution experiment: (1) ks decreases with dissolution;
388 (2) σ/ks increases slightly when dissolution starts and (3) then it decreases with greater
389 dissolution.

390

391 5.2 Sedimentary record of coccolith morphology: life-cycle vs. dissolution factors

392 Previous studies have evaluated changes in the calcification of Noëlaerhabdaceae
393 coccoliths in glacial-interglacial cycles through analyses of the coccolith mass and attributed
394 morphological variations mainly to water column nutrient availability and carbonate chemistry
395 parameters, related to the coccolithophores life-cycle (e.g., Beaufort et al., 2011). Su et al.
396 (2020) found that the environmental dynamics of the surface photic zone controlled
397 Noëlaerhabdaceae coccoliths' calcification in northern SCS (MD05-2904). Similarly, higher
398 calcite production recorded by increased coccolith mass has been attributed to the increased
399 $[CO_3^{2-}]$ in the surface water column in the South Indian Ocean and North Atlantic Ocean in
400 modern sediments (Beaufort et al., 2011). Dissolution effects were thought to be less likely
401 drivers of changes in the morphology of coccolith (Beaufort et al., 2011; Su et al., 2020), which
402 is a reasonable assumption for the coccoliths depositing in shallow sediments above the
403 lysocline. These interpretations are partially sustained by the findings of Beaufort et al. (2007),
404 who found no significant coccolith dissolution during the settling in sediment traps deployed
405 between 250 and 2500 m. The former study proposed that most of the dissolution occurs in the
406 euphotic zone and possibly in the guts of grazers, therefore, discarding the impact of bottom
407 water chemistry and/or post-burial processes on coccolithophore weight.

408 In our set of samples in the SCS, the RDA results show that mean thickness and length
409 significantly correlate to nitrate and phosphate at 50 m (Table 2). This observation agrees with
410 Jin et al. (2016), who found that biometric attributes of *E. huxleyi* correlated with nutrient
411 concentrations in the plankton samples in the ECS. Nutrient variables are important for
412 coccolithophore calcification (Raven and Crawford, 2012) and morphological parameters, at
413 least in species of the Noëlaerhabdaceae family (Båtvik et al., 1997; Pasche et al., 1998).
414 However, based on the extended evidence of our study, including carbonate chemistry at the
415 depth of the sediment samples in the SCS, we observe evidence that several of the
416 morphological parameters measured are not only influenced by primary biomineralization. Still,
417 abiogenic post- or syn-depositional processes override this signal in the sediment samples in this
418 region. The highest correlations between coccolith morphology, namely mean ks , volume, and
419 thickness, with the bottom water calcite saturation, Ω_{Ca} , indicates that the calcium carbonate
420 preservation conditions could strongly override some of the morphological parameters in fossil



421 coccoliths (Table 2, Fig. 5A). We suggest that the mean k_s of coccolith could be a potential proxy
422 for the carbonate dissolution in the bottom water, especially in sites near or below the
423 lysocline.

424 Carbonate dissolution may also happen within the shallow sediment (Sulpis et al., 2021;
425 Subhas et al., 2022). Based on our current dataset and using only the morphological variations,
426 we cannot distinguish where the dissolution happens at the time of deposition in the sediment
427 water interface, or post-burial in the first cms of the seafloor sediment. For the deep ocean
428 depositions with lower sedimentary rates, such as the deepest parts of the SCS (Huang and
429 Wang, 2006), the exposure time of particles to bottom water should be longer than that along
430 the continental slope. Thus, we suggest that the major dissolution in the deep SCS happens on
431 the sediment-water boundary instead of within pore water. Interestingly, the k_s of coccolith in
432 the surface sediment of the ECS are much lower, as low as 0.01 (Jin et al., 2019), than those in
433 our study, which is higher than 0.04. However, the k_s of coccolith during the laboratory
434 dissolution experiment performed by Jin et al. (2019; Fig. 9A in that study) show the same range
435 as our measurements. The ECS samples are from the continental shelf with high sedimentary
436 rates and organic carbon content (Jin et al., 2019). In these settings, the coccoliths continuously
437 dissolve after being buried within the first centimeters of the seafloor sediments in response to
438 organic matter remineralization and CO_2 release, resulting in a ~30-50 % decrease in coccolith
439 mass (Jin et al., 2019). Therefore, the sedimentary environment has to be individually evaluated
440 to understand which process is controlling the dissolution of coccolithophores at the seafloor.
441 More detailed work, such as in-situ pore water chemistry measurements, would be necessary
442 to fully reveal the fate of coccolith dissolutions in different burial scenarios (Holcová and
443 Scheiner, 2022).

444 Among all the morphological parameters, we find the mean k_s of coccolith as a more
445 robust dissolution proxy compared to the other measured morphological parameters. Firstly,
446 we observe a higher correlation coefficient between mean k_s of coccolith and Ω_{Ca} compared
447 with other morphological parameters. Secondly, although volume, mass, and thickness are also
448 highly correlated with Ω_{Ca} , these morphological parameters vary more with the feature of
449 different coccolithophores, including variations in coccolith circularity and cell sizes (Young and
450 Ziveri, 2000; Bolton et al., 2016). Thirdly, the thickness is a morphological pattern sensitive to
451 the upper ocean's preservation and surface ocean environmental conditions during
452 biomineralization (Table 2). Another important feature of k_s is its high sensitivity to dissolution.
453 As shown in Fig. 4, the k_s of coccolith have already begun to decrease even though the water
454 depths are only at ~2000 m, which is below the modern lysocline but above the CDD in the SCS
455 (Wang et al., 1995; Luo et al., 2018). Finally, the dissolution effects on morphological attributes



456 of mean ks agree well with the laboratory dissolution experiment, in which each subsample's
457 mean ks reflected different preservation stages (Fig. 3).

458 Despite a noticeable degree of uncertainty due to the mixing of life-cycle and post-
459 mortem signals in the sedimentary record, similar findings of calcite dissolution modifying
460 coccolith's morphology in waters at or below saturation suggest that the conclusions drawn
461 from the present study are not unique to the SCS. In the Sub-Antarctic and Antarctic zone,
462 dissolution signals affecting coccolithophores were manifested as a decrease in mass and distal
463 shield length of *E. huxleyi* coccoliths preserved in surface sediments (Vollmar et al., 2022; Rigual-
464 Hernández et al., 2020b). Based on this collective evidence, a key reasonable question could be,
465 “can the morphological variation of coccolith be employed to trace the evolution safely, or could
466 they be a good proxy for carbonate preservation”?

467

468 5.3. Implications for interpreting the downcore history of coccolithophore morphology

469 On longer time scales, the morphological variations of coccoliths have been employed
470 to trace coccolithophores evolutionary trend. Bolton et al. (2016) first measured the ks of
471 Noëlaerhabdaceae in the last 15 million years. They found that the decrease of coccolith ks
472 paralleled the reduction of atmospheric pCO₂ since the late Miocene and interpreted this as a
473 decrease in biomineralization. More recent works by Beaufort et al. (2022) and Jin et al. (2022b)
474 focused on the coccolithophore evolution over the last 2 million years by measuring coccolith
475 mass, highlighting the role of seasonality and local environments in the evolution and
476 production of Noëlaerhabdaceae. Similarly, Guitián et al. (2020) studied size trends across
477 different regions between Oligocene to the Early Miocene, concluding that cell size distribution
478 was controlled by multiple competing factors, with a strong selective pressure from CO₂ decline
479 a potential mechanism. This study examined dissolution by looking, among others, at the
480 fragmentation and etching of coccoliths and found that temporal trends in lith size distributions
481 were not significantly affected. This agrees with our observations since the mean length in SCS
482 surface sediments does not correlate with any saturation state related parameter. However,
483 Guitián et al. (2022), using a new calibration in the C-Calcita software that enables estimations
484 of coccolith thickness up to 3.1 microns, found that elliptical ks (kse) was inversely correlated
485 with the relative abundance of dissolution-resistant nannoliths. This was interpreted as a
486 dissolution control on the elliptical shape factors in coccolithophores between Oligocene and
487 Miocene, as it was found in our surface sediment samples. Therefore, we propose that for
488 studies focusing on coccolithophores evolutionary histories, it would be safer to select a shallow
489 sediment core with low organic carbon content, high clay content, and always lying above the
490 carbonate lysocline (Guitián et al., 2020).



491 One useful way to identify dissolution in these studies covering geological time scales
492 could be plotting the σ/ks against ks . If an increase of σ/ks is detected in the sediment coccolith
493 without any significant variations in coccolith assemblage or with an increase of dissolution-
494 resistant species (Gutián et al., 2022), it should be interpreted as a dissolution. Another way to
495 determine separate evolutionary/ecological influences on ks variations could be to measure the
496 ks of coccolith across a close spatial gradient which includes different depositional depths.
497 Significant variations in the morphological attributes of the fossil coccolithophores would likely
498 be caused by different saturation through time at different sites. Related to this last suggestion,
499 coupling downcore morphological assessment in coccolithophores with other calcareous
500 proxies measurements, such as size-normalized weight of planktic foraminiferal tests (Lohman,
501 1995; Broecker and Clark, 2001; Barker et al., 2002), which include recent advances in
502 morphological analyses in large microfossils (Iwasaki et al., 2015; 2019), may provide an even
503 more precise and safe quantitative estimates of past deep-carbonate chemistry parameters.

504 6. Summary

505 This study demonstrates, based on morphological attributes of *E. huxleyi* and
506 *Gephyrocapsa* spp. ($> 2 \mu\text{m}$), that dissolution effects primarily affect the morphology of
507 coccoliths preserved in the deep ocean. In the SCS surface sediments, bottom water Ω_{ca}
508 saturation plays a major role in the variation of the coccoliths' ks shape factor, which has the
509 potential, based on the current calibration, to quantitatively reconstruct past carbonate
510 dissolution changes. Our laboratory-controlled dissolution results show that the mean ks
511 decreased in response to increased amounts of corrosive solution. We propose the ratio σ/ks
512 vs. mean ks to evaluate the degree of dissolution (light, strong, or no dissolution) occurring in
513 the sedimentary record. A length-related dissolution pattern was also observed in the laboratory
514 and surface sediments, with small coccoliths more prone to suffer dissolution, increasing larger
515 coccolith specimens and affecting the assemblage composition. As in the laboratory experiment,
516 the coccolith's ks from surface sediments decreased with dissolution, and the σ/ks trajectory
517 reflected different dissolution stages. However, the σ/ks in surface sediment showed a more
518 complex response due to the natural variability of the surface sediment samples in terms of
519 geographical differences in multiple environmental factors. These findings demonstrate that,
520 despite the complexity of the carbonate system and ecological aspects, the coccoliths ks factor
521 allied to σ/ks ratio has potential as a dissolution proxy to track changes in the seafloor carbonate
522 saturation state. Although a stable proxy, the mean ks should be applied with caution,
523 particularly when applied to longer time scales, in which evolutionary trends might exert control
524 on morphological attributes of fossil coccolithophores.



525 Author contributions

526 AG, HZ, RHN and IHA conceived and designed the study. AG and HZ conducted the lab work and
527 sample analyses. AG, HZ and IHA performed the statistical analysis. AG, HZ and IHA wrote the
528 manuscript with substantial contributions from all co-authors.

529 Competing interests

530 The authors declare that they have no conflict of interest.

531 Data availability

532 Research data is available as supplementary material and in the Zenodo
533 (<https://doi.org/10.5281/zenodo.7271441>, Gerotto et al., 2022) and PANGAEA (pending doi)
534 data repositories.

535 Acknowledgments

536 This study was financed in part by the Coordenação de Aperfeiçoamento de Pessoal de Nível
537 Superior - Brasil (CAPES) - Finance Code 001 to A.G. and the ETH Core and Swiss National Science
538 Foundation (Award 200021_182070) funding to H. M. Stoll. Additional funding was provided by
539 the National Natural Science Foundation of China (grants 42188102 and 41930536) to C.L.
540 Thanks also to the International Ocean Discovery program for providing the sample used for the
541 dissolution experiment.

542 References

- 543 Archer, D., Winguth, A., Lea, D., and Mahowald, N. What caused the glacial/interglacial
544 atmospheric pCO₂ cycles? *Rev. Geophys.*, 38–2(1999), 159–189, 2000.
- 545 Barker, S., and Elderfield, H. Foraminiferal calcification response to glacial-interglacial changes
546 in atmospheric CO₂, *Science*, 297(5582), 833–836,
547 <https://doi.org/10.1126/science.1072815>, 2002.
- 548 Båtvik, H., Heimdal, B. R., Fagerbakke, K. M., Green, J. C. Effects of unbalanced nutrient regime
549 on coccolith morphology and size in *Emiliania huxleyi* (Prymnesiophyceae), *Eur. J.*
550 *Phycol.*, 32(2), 155–165, <https://doi.org/10.1080/09670269710001737089>, 1997.
- 551 Beaufort, L. Weight estimates of coccoliths using the optical properties (birefringence) of calcite,
552 *Micropaleontology*, 51, 289–297, <https://doi.org/10.2113/gsmicropal.51.4.289>, 2005.
- 553 Beaufort, L., Gally, Y., Suchéras-Marx, B., Ferrand, P., and Duboisset, J. A universal method for
554 measuring the thickness of microscopic calcite crystals, based on Bidirectional Circular
555 Polarization, *Biogeosciences*, 18 (3), 775–785, <https://doi.org/10.5194/bg-18-775-2021>,
556 2021.



- 557 Beaufort, L., Probert, I., De Garidel-Thoron, T., Bendif, E. M., Ruiz-Pino, D., Metzl, N., et al.
558 Sensitivity of coccolithophores to carbonate chemistry and ocean acidification, *Nature*,
559 476(7358), 80–83, <https://doi.org/10.1038/nature10295>, 2011.
- 560 Beaufort, L., Probert, I., and Buchet, N. Effects of acidification and primary production on
561 coccolith weight: Implications for carbonate transfer from the surface to the deep
562 ocean, *Geochem., Geophys., Geosy.*, 8(8), 1–18,
563 <https://doi.org/10.1029/2006GC001493>, 2007.
- 564 Beaufort, L., Bolton, C. T., Sarr, A. C. et al. Cyclic evolution of phytoplankton forced by changes
565 in tropical seasonality, *Nature*, 601, 79–84, [https://doi.org/10.1038/s41586-021-04195-](https://doi.org/10.1038/s41586-021-04195-7)
566 7, 2022.
- 567 Bollmann, J. Weight approximation of coccoliths using a circular polarizer and interference
568 colour derived retardation estimates – (The CPR Method), *Biogeosciences*, 11, 1899–
569 1910, <https://doi.org/10.5194/bg-11-1899-2014>, 2014.
- 570 Bollmann, J., Herrle, J. O. Morphological variation of *Emiliania huxleyi* and sea surface salinity,
571 *Earth Planet. Sc. Lett.*, 255(3-4), 273–288, <https://doi.org/10.1016/j.epsl.2006.12.029>,
572 2007.
- 573 Bolton, C. T., Hernández-Sánchez, M. T., Fuertes, M. Á., González-Lemos, S., Abrevaya, L.,
574 Mendez-Vicente, A., et al. Decrease in coccolithophore calcification and CO₂ since the
575 middle Miocene, *Nature Communications*, 7, 10284,
576 <https://doi.org/10.1038/ncomms10284>, 2016.
- 577 Bordiga, M., Bartol, M., Henderiks, J. Absolute nannofossil abundance estimates: 314
578 Quantifying the pros and cons of different techniques, *Rev. de Micropaleontol.*, 58, 155–
579 165, <https://doi:10.1016/j.revmic.2015.05.002>, 2015.
- 580 Broecker, W. S., and Clark, E. Glacial-to-Holocene Redistribution of Carbonate Ion in the Deep
581 Sea, *Science*, 294(5549), 2152–2155, <http://www.jstor.org/stable/3085356>, 2001.
- 582 Broerse, A. T. C., Ziveri, P., and Honjo, S. Coccolithophore (–CaCO₃) flux in the Sea of Okhotsk:
583 Seasonality, settling and alteration processes, *Mar. Micropaleontol.*, 39(1–4), 179–200,
584 [https://doi.org/10.1016/S0377-8398\(00\)00020-7](https://doi.org/10.1016/S0377-8398(00)00020-7), 2000.
- 585 Buiteveld, H. A model for calculation of diffuse light attenuation (PAR) and Secchi depth, *Neth.*
586 *J. Aquat. Ecol.*, 29, 55–65, <https://doi.org/10.1007/BF02061789>, 1995.
- 587 Charalampopoulou, A., Poulton, A. J., Bakker, D. C. E., Lucas, M. I., Stinchcombe, M. C., Tyrrell,
588 T. Environmental drivers of coccolithophore abundance and calcification across Drake
589 Passage (Southern Ocean), *Biogeosciences*, 13, 5917–5935, [https://doi.org/10.5194/bg-](https://doi.org/10.5194/bg-13-5917-2016)
590 13-5917-2016, 2016.



- 591 Chen, C. T. A., Wang, S. L., Chou, W. C., and Sheu, D. D. Carbonate chemistry and projected future
592 changes in pH and CaCO₃ saturation state of the South China Sea, *Mar. Chem.*, 101(3–
593 4), 277–305, <https://doi.org/10.1016/j.marchem.2006.01.007>, 2006.
- 594 Chen, C. T. A., Wang, S. L., Wang, B. J., and Pai, S. C. Nutrient budgets for the South China sea
595 basin, *Mar. Chem.*, 75(4), 281–300, [https://doi.org/10.1016/S0304-4203\(01\)00041-X](https://doi.org/10.1016/S0304-4203(01)00041-X),
596 2001.
- 597 Chen, Y. L. L. Spatial and seasonal variations of nitrate-based new production and primary
598 production in the South China Sea, *Deep-Sea Res. Pt. I*, 52(2), 319–340,
599 <https://doi.org/10.1016/j.dsr.2004.11.001>, 2005.
- 600 Chen, Y. L. L., Chen, H. Y., and Chung, C. W. Seasonal variability of coccolithophore abundance
601 and assemblage in the northern South China Sea, *Deep-Sea Res. Pt. II: Top. Stud.*
602 *Oceanogr.*, 54(14–15), 1617–1633, <https://doi.org/10.1016/j.dsr2.2007.05.005>, 2007.
- 603 Chou, W. C., Sheu, D. D., Lee, B. S., Tseng, C. M., Chen, C. T. A., Wang, S. L., and Wong, G. T. F.
604 Depth distributions of alkalinity, TCO₂ and δ^{13} CTCO₂ at SEATS time-series site in the
605 northern South China Sea, *Deep-Sea Res. Pt. II: Top. Stud. Oceanogr.*, 54(14–15), 1469–
606 1485, <https://doi.org/10.1016/j.dsr2.2007.05.002>, 2007.
- 607 Conkright, M. E., Locarnini, R. A., Garcia, H. E., O’Brien, T. D., Boyer, T. P., Stephens, C., Antonov,
608 J. I. *World Ocean Atlas 2001: Objective Analyses, Data Statistics, and Figures*, CD-ROM
609 Documentation. National Oceanographic Data Center, Silver Spring, MD, 17 pp, 2002.
- 610 Emerson, S. R., and Archer, D. Calcium carbonate preservation in the ocean. *Philos. Tr. R. Soc. S-*
611 *A.*, 331(1616), 29–40, <https://doi.org/10.1098/rsta.1990.0054>, 1990.
- 612 Eppley, R. W., Rogers, J. N., and McCarthy, J. J. Half-saturation constants for uptake of nitrate
613 and ammonia, *Limnol. Oceanogr.*, 14(6), 912–920,
614 <https://doi.org/10.4319/lo.1969.14.6.0912>, 1969.
- 615 Feldmeijer, W., Metcalfe, B., Scussolini, P., and Arthur, K. The effect of chemical pretreatment of
616 sediment upon foraminiferal-based proxies, *Geochem., Geophys., Geosy.*, 14(10), 3996–
617 4014, <https://doi.org/10.1002/ggge.20233>, 2013.
- 618 Fernando, A. G. S., Peleo-Alampay, A. M., Lucero, E. S., and Wiesner, M. G. Surface sediment
619 distribution of *Florisphaera profunda* in the South China Sea: an effect of dissolution? *J.*
620 *Nannoplankton Res.*, 29(2), 102–07, 2007a.
- 621 Fernando, A. G. S., Peleo-Alampay, A. M., and Wiesner, M. G. Calcareous nannofossils in surface
622 sediments of the eastern and western South China Sea, *Mar. Micropaleontol.*, 66, 1–26,
623 <https://doi.org/10.1016/j.marmicro.2007.07.003>, 2007b.



- 624 Flores, J. A., Marino, M., Sierro, F. J., Hodell, D. A., and Charles, C. D. Calcareous plankton
625 dissolution pattern and coccolithophore assemblages during the last 600 kyr at ODP Site
626 1089 (Cape Basin, South Atlantic): Paleocceanographic implications. *Palaeogeogr*
627 *Palaeocl.*, 196(3–4), 409–426, [https://doi.org/10.1016/S0031-0182\(03\)00467-X](https://doi.org/10.1016/S0031-0182(03)00467-X), 2003.
- 628 Fuertes, M. Á., Flores, J. A., and Sierro, F. J. The use of circularly polarized light for biometry,
629 identification and estimation of mass of coccoliths, *Mar. Micropaleontol.*, 113, 44–55,
630 <https://doi.org/10.1016/j.marmicro.2014.08.007>, 2014.
- 631 Gerotto, A., Zhang, H., Nagai, R. H., Stoll, H. M., Figueira, R. C. L., Chuanlian, L., Hernández-
632 Almeida, I. Morphological measurements of coccoliths from surface samples of South
633 China Sea, Zenodo [data set], <https://doi.org/10.5281/zenodo.7271441>, 2022.
- 634 González-Lemos, S., Guitián, J., Fuertes, M. Á., Flores, J. A., and Stoll, H. M. Technical note: An
635 empirical method for absolute calibration of coccolith thickness, *Biogeosciences*, 15(4),
636 1079–1091, <https://doi.org/10.5194/bg-15-1079-2018>, 2018.
- 637 Goyet, C., Healy, R. J., and Ryan, J. P. Global distribution of total inorganic carbon and total
638 alkalinity below the deepest winter mixed layer depths. ORNL/CDIAC-127, NDP-076.
639 Carbon Dioxide Information Analysis Center, Oak Ridge National Laboratory, U.S.
640 Department of Energy, Oak Ridge, Tennessee, 2000.
- 641 Guitián, J., Dunkley Jones, T., Hernández-Almeida, I., Löffel, T., and Stoll, H. M. Adaptations of
642 coccolithophore size to selective pressures during the Oligocene to Early Miocene high
643 CO₂ world, *Paleoceanogr. and Paleoclimatology*, 35(12), e2020PA003918,
644 <https://doi.org/10.1029/2020PA003918>, 2020.
- 645 Guitián, J., Fuertes, M. Á., Flores, J. A., Hernández-Almeida, I., and Stoll, H. Variation in
646 calcification of Reticulofenestra coccoliths over the Oligocene-Early Miocene, *Biogeosci.*
647 *Discuss.*, 1-17, <https://doi.org/10.5194/bg-2022-66>, 2022.
- 648 Hammer, Ø., Harper, D. A. T., Ryan, P. D. PAST: Paleontological Statistics Software Package for
649 Education and Data Analysis, *Palaeontol. Electron.*, 4(1), 1–9,
650 doi.org/10.1016/j.bcp.2008.05.025, 2001.
- 651 Hay, W. W. Carbonate fluxes and calcareous nannoplankton.
652 H. Thierstein, J. Young (Eds.), *Coccolithophores: From Molecular Processes to Global*
653 *Impact*, Springer, Berlin (2004), pp. 509-528, 2004.
- 654 Henderiks, J., and Pagani, M. Refining ancient carbon dioxide estimates: Significance of
655 coccolithophore cell size for alkenone-based pCO₂ records, *Paleoceanography*, 22(3), 1–
656 12, <https://doi.org/10.1029/2006PA001399>, 2007.



- 657 Hernández, A. S. R., Trull, T. W., Nodder, S. D., Flores, J. A., Bostock, H., Abrantes, F., et al.
658 Coccolithophore biodiversity controls carbonate export in the Southern Ocean,
659 *Biogeosciences*, 17(1), 245–263, <https://doi.org/10.5194/bg-17-245-2020>, 2020.
- 660 Holcová, K., and Scheiner, F. An experimental study on post-mortem dissolution and overgrowth
661 processes affecting coccolith assemblages: A rapid and complex process, *Geobiology*,
662 (September), 1–17, <https://doi.org/10.1111/gbi.12528>, 2022.
- 663 Hönisch, B., Ridgwell, A., Schmidt, D. N., Thomas, E., Gibbs, S. J., Sluijs, A., et al. The geological
664 record of ocean acidification, *Science*, 335(6072), 1058–1063,
665 <https://doi.org/10.1126/science.1208277>, 2012.
- 666 Huang, W., and Wang, P. Sediment mass and distribution in the South China Sea since the
667 Oligocene. *Sci. China Ser. D Earth Sci.* 49, 1147–1155. [https://doi:10.1007/s11430-006-](https://doi:10.1007/s11430-006-2019-4)
668 2019-4, 2006.
- 669 Iglesias-Rodriguez, M. D., Halloran, P. R., Rickaby, R. E. M., Hall, I. R., Colmenero-Hidalgo, E.,
670 Gittins, J. R., et al. Phytoplankton calcification in a high-CO₂ world, *Science*, 320(5874),
671 336–340, <https://doi.org/10.1126/science.1154122>, 2008.
- 672 IPCC: Climate Change and Land: an IPCC special report on climate change, desertification, land
673 degradation, sustainable land management, food security, and greenhouse gas fluxes in
674 terrestrial ecosystems [P.R. Shukla, J. Skea, E. Calvo Buendia, V. Masson-Delmotte, H.-
675 O. Pörtner, D. C. Roberts, P. Zhai, R. Slade, S. Connors, R. van Diemen, M. Ferrat, E.
676 Haughey, S. Luz, S. Neogi, M. Pathak, J. Petzold, J. Portugal Pereira, P. Vyas, E. Huntley,
677 K. Kissick, M. Belkacemi, J. Malley, (eds.)]. In press, 2019.
- 678 Iwasaki, S., Kimoto, K., Okazaki, Y., and Ikehara, M. Micro-CT Scanning of Tests of Three Planktic
679 Foraminiferal Species to Clarify Dissolution Process and Progress, *Geochem., Geophys.,*
680 *Geosy.*, 20(12), 6051-6065, <https://doi.org/10.1029/2019GC008456>, 2019.
- 681 Iwasaki, S., Kimoto, K., Sasaki, O., Kano, H., Honda, M. C., and Okazaki, Y. Observation of the
682 dissolution process of *Globigerina bulloides* tests (planktic foraminifera) by X-ray
683 microcomputed tomography, *Paleoceanography*, 30(4), 317-331,
684 <https://doi.org/10.1002/2014PA002639>, 2015.
- 685 Johnsen, S. L., and Bollmann, J. Segmentation, retardation and mass approximation of
686 birefringent particles on a standard light microscope, *J. Microsc.*, 280, 30-50,
687 <https://doi.org/10.1111/jmi.12932>, 2020.
- 688 Jin, X., Liu, C., Poulton, A. J., Dai, M., and Guo, X. Coccolithophore responses to environmental
689 variability in the South China Sea: Species composition and calcite content,
690 *Biogeosciences*, 13(16), 4843–4861, <https://doi.org/10.5194/bg-13-4843-2016>, 2016.



- 691 Jin, X., Liu, C., Xu, J., and Guo, X. Coccolithophore Abundance, Degree of Calcification, and Their
692 Contribution to Particulate Inorganic Carbon in the South China Sea, *J. Geophys. Res-*
693 *Biogeo.*, 127(4), e2021JG006657, <https://doi.org/10.1029/2021JG006657>, 2022a.
- 694 Jin, X., Liu, C., and Zhang, H. Coccolith morphological and assemblage responses to dissolution
695 in the recent sediments of the East China Sea, *Mar. Micropaleontol.*, 152(January 2018),
696 101709, <https://doi.org/10.1016/j.marmicro.2018.09.001>, 2019.
- 697 Jin, X., Ma, W., and Liu, C. Origin of the long-term increase in coccolith size and its implication
698 for carbon cycle and climate over the past 2 Myr, *Quaternary Sci. Rev.*, 290, 107642,
699 <https://doi.org/10.1016/j.quascirev.2022.107642>, 2022b.
- 700 Le J., and Shackleton, N. J. Carbonate dissolution fluctuations in the western equatorial Pacific
701 during the late Quaternary, *Paleoceanography*, 7, 21–42,
702 <https://doi.org/10.1029/91PA02854>, 1992.
- 703 Libes, S. M. An Introduction to Marine Biogeochemistry, 2nd ed. Burlington, MA:
704 Academic Press Noone, K., Sumaila, R.; Diaz R.J. (eds) 2009. Valuing the
705 Oceans, Stockholm Environmental Institute, 2009.
- 706 Lin, J., Lee, Z., Ondrusek, M., and Du, K. Remote sensing of normalized diffuse
707 attenuation coefficient of downwelling irradiance, *J. Geophys. Res-Oceans*, 121(9),
708 6717-6730, <https://doi.org/10.1002/2016JC011895>, 2016.
- 709 Liu, J., Xiang, R., Chen, M., Chen, Z., Yan, W., and Liu, F. Influence of the Kuroshio current
710 intrusion on depositional environment in the Northern South China Sea: Evidence from
711 surface sediment records, *Mar. Geol.*, 285(1–4), 59–68,
712 <https://doi.org/10.1016/j.margeo.2011.05.010>, 2011.
- 713 Lohman, G.P. A model for variation in the chemistry of planktonic foraminifera due to secondary
714 calcification and selective dissolution, *Paleoceanogr. Paleoclimatol.*, 10(3), 445-457,
715 <https://doi.org/10.1029/95PA00059>, 1995.
- 716 Luo, Y., Kienast, M., and Boudreau, B. P. Invariance of the carbonate chemistry of the South
717 China Sea from the glacial period to the Holocene and its implications to the Pacific
718 Ocean carbonate system, *Earth Planet. Sci. Lett.*, 492, 112–120,
719 <https://doi.org/10.1016/j.epsl.2018.04.005>, 2018.
- 720 Murtugudde, R., Beauchamp, J., McClain, C. R., Lewis, M., and Busalacchi, A. Effects of
721 penetrative radiation on the upper tropical ocean circulation, *J. Climate*, 15(5), 470-486,
722 [https://doi.org/10.1175/1520-0442\(2002\)015<0470:EOPROT>2.0.CO;2](https://doi.org/10.1175/1520-0442(2002)015<0470:EOPROT>2.0.CO;2), 2002.
- 723 Paasche, E. Roles of nitrogen and phosphorus in coccolith formation in *Emiliania huxleyi*
724 (Prymnesiophyceae), *Eur. J. Phycol.*, 33(1), 33-42,
725 <https://doi.org/10.1080/09670269810001736513>, 1998.



- 726 Pälike, H., Lyle, M. W., Nishi, H., Raffi, I., Ridgwell, A., Gamage, K., et al. A Cenozoic record of the
727 equatorial Pacific carbonate compensation depth, *Nature*, 488(7413), 609–614,
728 <https://doi.org/10.1038/nature11360>, 2012.
- 729 Pälike, H., Norris, R. D., Herrle, J. O., Wilson, P. A., Helen, K., Lear, C. H., et al. The Heartbeat of
730 the Oligocene Climate System, *Science*, 314(5807), 1894–1898,
731 <https://www.jstor.org/stable/20035092>, 2006.
- 732 Pierrot, D., Lewis, E., and Wallace, D. W. R. MS Excel Program Developed for CO₂ System
733 Calculations - version 2.1. ORNL/CDIAC-105a. Carbon Dioxide Information Analysis
734 Center, Oak Ridge National Laboratory, U.S. Department of Energy, Oak Ridge,
735 Tennessee, https://doi.org/10.3334/CDIAC/otg.CO2SYS_XLS_CDIAC105a, 2012.
- 736 Pinxian, W., Qiubao, M., Yunhua, B., and Wenke, F. Planktonic Foraminifera in the Continental
737 Slope of the Northern South China Sea during the Last 130,000 Years and Their Paleo-
738 Oceanographic Implications, *Acta Geol. Sin-Engl.*, 60(3), 1–11,
739 <https://doi.org/10.1111/j.1755-6724.1986.mp60003001.x>, 1986.
- 740 Qu, T., Girton, J. B., and Whitehead, J. A. Deepwater overflow through Luzon Strait, *J. Geophys.*
741 *Res.*, 111(C1), C01002, <https://doi.org/10.1029/2005JC003139>, 2006.
- 742 Qu, T., Song, Y. T., and Yamagata, T. An introduction to the South China Sea throughflow: Its
743 dynamics, variability, and application for climate, *Dynam. Atmos. Oceans*, 47(1–3), 3–
744 14, <https://doi.org/10.1016/j.dynatmoce.2008.05.001>, 2009.
- 745 Rae, J. W. B., Zhang, Y. G., Liu, X., Foster, G. L., Stoll, H. M., and Whiteford, R. D. M. Atmospheric
746 CO₂ over the Past 66 Million Years from Marine Archives, *Annu. Rev. Earth Pl. Sc.*, 49,
747 609–641, <https://doi.org/10.1146/annurev-earth-082420-063026>, 2021.
- 748 Raven, J. A., and Crawford, K. Environmental controls on coccolithophore calcification. *Mar. Ecol.*
749 *Prog. Ser.*, 470, 137–166. <http://www.jstor.org/stable/24876210>, 2012.
- 750 Rickaby, R. E. M., Bard, E., Sonzogni, C., Rostek, F., Beaufort, L., Barker, S., et al. Coccolith
751 chemistry reveals secular variations in the global ocean carbon cycle? *Earth Planet. Sci.*
752 *Lett.*, 253(1–2), 83–95, <https://doi.org/10.1016/j.epsl.2006.10.016>, 2007.
- 753 Ridgwell, A., and Zeebe, R. E. The role of the global carbonate cycle in the regulation and
754 evolution of the Earth system, *Earth Planet. Sci. Lett.*, 234(3–4), 299–315,
755 <https://doi.org/10.1016/j.epsl.2005.03.006>, 2005.
- 756 Riebesell, U., Zondervan, I., Rost, B., Tortell, P. D., Zeebe, R. E., and Morel, F. M. M. Reduced
757 calcification of marine plankton in response to increased atmospheric CO₂, *Nature*, 407,
758 364–367, <https://doi.org/10.1038/35030078>, 2000.
- 759 Rigual-Hernández, A. S., Sánchez-Santos, J. M., Eriksen, R., Moy, A. D., Sierro, F. J., Flores, J. A.,
760 et al. Limited variability in the phytoplankton *Emiliania huxleyi* since the pre-industrial



- 761 era in the Subantarctic Southern Ocean. *Anthropocene*, 31, 100254,
762 <https://doi.org/10.1016/j.ancene.2020.100254>, 2020b.
- 763 Rigual Hernández, A. S., Trull, T. W., Nodder, S. D., Flores, J. A., Bostock, H., Abrantes, F., Eriksen,
764 R.S., Sierro, F. J., Davies, D. M., Ballegeer, A.-M., Fuertes, M. A., and Northcote, L. C.
765 Coccolithophore biodiversity controls carbonate export in the Southern Ocean,
766 *Biogeosciences*, 17, 245–263, <https://doi.org/10.5194/bg-17-245-2020>, 2020a.
- 767 Roth, P. H., and Berger, W. H. Distribution and dissolution of coccoliths in the South and Central
768 Pacific. Sliter W.V., Be´ A.W.H., Berger W.H. (Eds.), *Dissolution of Deep-Sea*
769 *Carbonates*, Cushman Foundation Foraminiferal Research, Spec. Publ., N. 13, pp. 87-
770 113, 1975.
- 771 Roth, P. H., and Coulbourn, W. T. Floral and solution patterns of coccoliths in surface sediments
772 of the North Pacific. *Marine Micropaleontology*, 7(1), 1-52,
773 [https://doi.org/10.1016/0377-8398\(82\)90014-7](https://doi.org/10.1016/0377-8398(82)90014-7), 1982.
- 774 Sarmiento, J. L., Gruber, N. *Ocean Biogeochemical dynamics*. Princeton, NJ, Woodstock:
775 Princeton University Press. 528 pp, 2006.
- 776 Schlitzer, R. Ocean data View. Available at:<<http://odv.awi.de>>, 2019.
- 777 Stoll, H. M., Ziveri, P. Separation of monospecific and restricted coccolith assemblages from
778 sediments using differential settling velocity, *Mar. Micropaleontol.*, 46(1–2), 209-221,
779 [https://doi.org/10.1016/S0377-8398\(02\)00040-3](https://doi.org/10.1016/S0377-8398(02)00040-3), 2002.
- 780 Su, X., Liu, C., and Beaufort, L. Late Quaternary coccolith weight variations in the northern South
781 China Sea and their environmental controls, *Mar. Micropaleontol.*, 154, 101798,
782 <https://doi.org/10.1016/j.marmicro.2019.101798>, 2020.
- 783 Subhas, A. V., Dong, S., Naviaux, J. D., Rollins, N. E., Ziveri, P., Gray, W., et al. Shallow Calcium
784 Carbonate Cycling in the North Pacific Ocean, *Global Biogeochem. Cy.*, 36(5), 1–22,
785 <https://doi.org/10.1029/2022GB007388>, 2022.
- 786 Sulpis, O., Boudreau, B. P., Mucci, A., Jenkins, C., Trossman, D. S., Arbic, B. K., and Key, R. M.
787 Current CaCO₃ dissolution at the seafloor caused by anthropogenic CO₂, *P. Natl. Acad.*
788 *Sci. USA*, 115(46), 11700–11705, <https://doi.org/10.1073/pnas.1804250115>, 2018.
- 789 Sulpis, O., Jeansson E., Dinauer A., Lauvset, S. K., and Middelburg, J. J. Calcium carbonate
790 dissolution patterns in the ocean, *Nat. Geosci.*, 14(6), 423–428,
791 <http://dx.doi.org/10.1038/s41561-021-00743-y>, 2021.
- 792 Thunell, R. C., Qingmin, M., Calvert, S. E., and Pedersen, T. F. Glacial-Holocene Biogenic
793 Sedimentation Patterns in the South China Sea: Productivity Variations and Surface
794 Water pCO₂, *Paleoceanography*, 7(2), 143–162, <https://doi.org/10.1029/92PA00278>,
795 1992.



- 796 Tian, J., Huang, E., and Pak, D. K. East Asian winter monsoon variability over the last glacial cycle:
797 Insights from a latitudinal sea-surface temperature gradient across the South China Sea,
798 *Palaeogeogr. Palaeocl.*, 292(1–2), 319–324,
799 <https://doi.org/10.1016/j.palaeo.2010.04.005>, 2010.
- 800 USGCRP. Climate Science Special Report: Fourth National Climate Assessment, Volume I
801 [Wuebbles, D.J., D.W. Fahey, K.A. Hibbard, D.J. Dokken, B.C. Stewart, and T.K. Maycock
802 (eds.)]. U.S. Global Change Research Program, Washington, DC, USA, 470 pp., 2017.
- 803 Vollmar, N. M., Baumann, K. H., Saavedra-Pellitero, M., and Hernández-Almeida, I. Distribution
804 of coccoliths in surface sediments across the Drake Passage and calcification of *Emiliania*
805 *huxleyi* morphotypes, *Biogeosciences*, 19(3), 585–612, [https://doi.org/10.5194/bg-19-](https://doi.org/10.5194/bg-19-585-2022)
806 585-2022, 2022.
- 807 Wan, S., and Jian, Z. Deep water exchanges between the South China Sea and the Pacific since
808 the last glacial period, *Paleoceanography*, 29(12), 1162–1178,
809 <https://doi.org/10.1002/2013PA002578>, 2014.
- 810 Wan, S., Jian, Z., and Dang, H. Deep Hydrography of the South China Sea and Deep Water
811 Circulation in the Pacific Since the Last Glacial Maximum, *Geochem., Geophys., Geosy.*,
812 19(5), 1447–1463, <https://doi.org/10.1029/2017GC007377>, 2018.
- 813 Wan, S., Jian, Z., Gong, X., Dang, H., Wu, J., and Qiao, P. Deep water [CO₃²⁻] and circulation in
814 the south China sea over the last glacial cycle, *Quat. Sci. Rev.*, 243, 106499,
815 <https://doi.org/10.1016/j.quascirev.2020.106499>, 2020.
- 816 Wang, N., Huang, B.-Q., and Li, H. Deep-water carbonate dissolution in the northern South China
817 Sea during Marine Isotope Stage 3, *J. Palaeogeogr.*, 5(1), 100–107,
818 <https://doi.org/10.1016/j.jop.2015.11.004>, 2016.
- 819 Wang, P., Li, Q., and Dai, M. The South China Sea Deep: Introduction, *Deep-Sea Res. Pt. II: Top.*
820 *Stud. Oceanogr.*, 122, 1-5, <https://doi.org/10.1016/j.dsr2.2015.11.004>, 2015.
- 821 Wang, P., Wang, L., Bian, Y., and Jian, Z. Late Quaternary paleoceanography of the South China
822 Sea: surface circulation and carbonate cycles, *Mar. Geol.*, 127(1–4), 145–165,
823 [https://doi.org/10.1016/0025-3227\(95\)00008-M](https://doi.org/10.1016/0025-3227(95)00008-M), 1995.
- 824 Wang, P. X., and Li, Q. Y. *The South China Sea: Paleoceanography and Sedimentology*. Springer,
825 Berlin, Heidelberg, New York, p. 506, 2009.
- 826 Young, J. R., and Ziveri, P. Calculation of coccolith volume and its use in calibration of carbonate
827 flux estimates, *Deep-Sea Res. Pt. II: Top. Stud. Oceanogr.*, 47(9–11), 1679–1700,
828 [https://doi.org/10.1016/S0967-0645\(00\)00003-5](https://doi.org/10.1016/S0967-0645(00)00003-5), 2000.



- 829 Yu, J., and Elderfield, H. Benthic foraminiferal B/Ca ratios reflect deep water carbonate
830 saturation state, *Earth Planet. Sci. Lett.*, 258(1–2), 73–86,
831 <https://doi.org/10.1016/j.epsl.2007.03.025>, 2007.
- 832 Yu, J., Menviel, L., Jin, Z. D., Thornalley, D. J. R., S. Barker, S., Marino, G., et al. Sequestration of
833 carbon in the deep Atlantic during the last glaciation, *Nat. Geosci.*, 9, 319–324,
834 <https://doi.org/10.1038/ngeo2657>, 2016.
- 835 Zachos, J. C., Röhl, U., Schellenberg, S. A., Sluijs, A., Hodell, D. A., Kelly, D. C., et al. Paleoclimate:
836 Rapid acidification of the ocean during the paleocene-eocene thermal maximum,
837 *Science*, 308(5728), 1611–1615, <https://doi.org/10.1126/science.1109004>, 2005.
- 838 Zhang, H., Liu, C., Jin, X., Shi, J., Zhao, S., and Jian, Z. Dynamics of primary productivity in the
839 northern South China Sea over the past 24,000 years, *Geochem., Geophys., Geosy.*,
840 17(12), 4878–4891, <https://doi.org/10.1002/2016GC006602>, 2016.

841